

Phase diagram and coarsening dynamics in dry apolar active nematics with reciprocal local alignment

Arpan Sinha^{1,2,*} and Debasish Chaudhuri^{1,2,†}

¹*Institute of Physics, Sachivalaya Marg, Bhubaneswar 751005, India*

²*Homi Bhabha National Institute, Anushaktinagar, Mumbai 400094, India*

Using the Lebwohl-Lasher interaction for reciprocal local alignment, we present a comprehensive phase diagram for a dry, apolar, active nematic system using its stochastic dynamics. The nematic-isotropic transition in this system is first-order and fluctuation-dominated. Our phase diagram identifies three distinct regions based on activity and orientational noise relative to alignment strength: a homogeneous isotropic phase, a nematic phase with giant density fluctuations, and a coexistence region. Using mean-field analysis and hydrodynamic theory, we demonstrate that reciprocal interactions lead to a density fluctuation-induced first-order transition and derive a phase boundary consistent with numerical results. Quenching from the isotropic to nematic phase reveals coarsening dynamics with nematic ordering preceding particle clustering and similar scaling behaviors for density and nematic fields, exhibiting dynamic exponents between 2 and 3.

1. Introduction

Active nematics represent a fascinating class of nonequilibrium systems characterized by the collective motion and organization of self-propelled entities [1–6]. Inspired by a myriad of biological systems, ranging from the dynamic organization of the cytoskeleton within cells to the emergent behaviors observed in tissues and even granular materials, active nematics have emerged as a pivotal area of study at the interface of physics, biology, and materials science [3, 4, 7–9]. At the heart of active systems lies the concept of self-propulsion, where individual constituents continually convert internal energy into directed motion. This intrinsic activity, prevalent in biological systems such as motile cells and bacterial colonies, fuels a rich array of dynamic phenomena, including the spontaneous formation of orientational order, collective motion, and the emergence of complex spatiotemporal patterns [4, 7, 8]. Moreover, active nematics find analogs in nonliving systems, including vibrated granular matter and artificial microswimmers suspended in fluids. The last few decades have seen tremendous progress in understanding their collective properties and phase behaviors [1–4, 10–13].

In dry active matter, self-propelled particles (SPP) with local alignment display order-disorder transition coupled with density fluctuations. Consideration of ferromagnetic alignment of the active heading directions of individual propulsion led to flocking and persistent motion of the flocks. This was demonstrated in the celebrated Vicsek model and its variants and described by the Toner-Tu theory of coupled orientation and density fields [4, 14–17]. Numerical studies of polar rods with volume exclusion showed nematic alignment and clustering [18], and a related simplified model led to system-spanning clusters [19]. A Boltzmann-Landau-Ginzburg

kinetic theory approach, based on a Vicsek-like model of active nematics, produced hydrodynamic equations consistent with previous findings [2–4, 10, 11, 20]. In certain systems, alignment results from physical processes such as actual collisions between active elements [18, 21, 22]. Other instances involve effective interactions mediated by non-equilibrium mechanisms like complex biochemical signaling or visual and cognitive processes [23–25]. The former alignments are characterized by reciprocal interactions, while non-reciprocal rules often describe the latter [26–28]. In equilibrium systems, microscopic details are typically considered irrelevant to emergent macroscopic properties if the models share symmetries and conservation laws. However, recent studies on aligning active particles with short-range interactions, be it vectorial or nematic active matter, revealed that microscopic implementations in the form of reciprocity and additivity can influence macroscopic behaviors [23], e.g., leading to first-order or critical order-disorder transition in active apolar nematics in the presence or absence of reciprocity [29].

SPPs can lose their overall polarity when there are rapid reversals in the self-propulsion direction. In active nematics, particles spontaneously align along an axis $\hat{\mathbf{n}}$ with a $\hat{\mathbf{n}} \rightarrow -\hat{\mathbf{n}}$ symmetry [1, 2, 12, 20, 30–32]. Examples of such systems include colliding elongated objects [18, 19, 33], migrating cells [34, 35], cytoskeletal filaments [36], certain direction-reversing bacteria [37–41], and vibrated granular rods [21, 22]. Even at high activity levels, the apolar nature of the particles results in zero macroscopic velocity. Intriguingly, the collective properties of these apolar SPPs still show a clear dependence on activity, as orientational fluctuations drive particle current [2, 10–12, 20, 30].

In this paper, we consider a dry, apolar, active nematics model using a reciprocal additive alignment interaction between local neighbors. An earlier on-lattice implementation using the Lebwohl-Lasher potential of alignment [42] found a fluctuation-dominated phase separation associated with the ordering transition [30]. Our earlier off-lattice calculation of SPPs at a fixed activity

* arpan.s@iopb.res.in

† debc@iopb.res.in

demonstrated a clear first-order nematic-isotropic (NI) transition with increasing orientational noise [29].

In this paper, we present a comprehensive phase diagram as a function of changing activity and relative orientational noise with respect to the alignment strength. It shows three different parameter regimes characterized by (i) a homogeneous isotropic phase, (ii) a nematically aligned phase with significant density fluctuations, and (iii) a coexistence of nematic and isotropic in the presence of the largest density fluctuations. The order-disorder transition remains fluctuation-dominated and first-order across all parameter regimes. Using a mean-field hydrodynamic argument, we obtain an analytic prediction for the phase boundary that shows reasonable agreement with our numerical results. Our primary contribution is this direct calculation of the detailed phase diagram.

Moreover, we study the phase ordering dynamics after a deep quench from isotropic to nematic phase. The stochastic simulations show dynamical scaling for density and nematic fields, with similar scaling exponents with values bounded between non-conserved and conserved dynamics consistent with earlier hydrodynamic calculations [43]. We observe a delay in particle clustering dynamics relative to nematic ordering, with the delay time controlled by the depth of the quench. Our second main contribution is the direct calculation of phase ordering using stochastic simulations.

The rest of the paper is structured as follows: Section 2 details the model of dry active nematic with reciprocal alignment. Section 3 presents the comprehensive phase diagram. Section 4 describes the mean field hydrodynamic analysis, explaining the phase boundaries and the nature of the nematic-isotropic transition. We then explore the coarsening of nematic order and density field in Section 5. Finally, in Section 6, we conclude by summarizing our main results and presenting an outlook.

2. Model

In this study, we explore how N dry active apolar particles align collectively in a nematic manner in a two-dimensional (2D) area $A = L \times L$. With a fixed active speed v_0 , we describe the particles' microstate as $\{\mathbf{r}_i, \mathbf{u}_i, q_i\}$, where \mathbf{r}_i denotes position, \mathbf{u}_i signifies velocity, and q_i represents orientation. The evolution of particle positions unfolds as:

$$\mathbf{r}_i(t + dt) = \mathbf{r}_i(t) + q_i v_0 \mathbf{u}_i dt. \quad (1)$$

We adopt periodic boundary conditions. The polarity $q_i = \pm 1$ is randomly assigned with equal probability to model apolar particles. The heading direction $\mathbf{u}_i = (\cos \theta_i, \sin \theta_i)$ evolves along with the angle θ_i with respect to the x -axis. Dynamics are governed by a competition between inter-particle alignment and orientational noise. In active nematics, alignment interactions are designed to make neighboring particles' heading directions parallel or anti-parallel with equal likelihood.

We examine the interaction of particle heading directions using the Lebwohl-Lasher potential [30, 42]:

$$U = -J \sum_{\langle ij \rangle} \cos[2(\theta_i - \theta_j)] \quad (2)$$

within a cutoff distance r_c determining the interaction range $r_{ij} = |\mathbf{r}_i - \mathbf{r}_j| < r_c$, and setting the unit of length. Following the Ito convention, the orientational Brownian motion of $\mathbf{u}_i(\theta_i)$ is governed by:

$$\theta_i(t + dt) = \theta_i(t) - \mu(\partial U / \partial \theta_i) dt + \sqrt{2D_r} dB_i(t). \quad (3)$$

Here, μ represents mobility, D_r is the rotational diffusion constant, and dB_i is a Gaussian process with zero mean and correlation $\langle dB_i dB_j \rangle = \delta_{ij} dt$. These equations depict persistent motion for a free particle, where D_r determines the persistence time $\tau_p = D_r^{-1}$, setting the unit of time. The model illustrates apolar particles aligning nematically with strength $J > 0$. It is important to note that the torque experienced by a particle pair i, j is equal and opposite to each other.

Employing the Euler-Maruyama scheme, we perform direct numerical simulations by integrating Eq.(1) and (3) using $dt = 7 \times 10^{-4} D_r^{-1}$. Care is taken so that $v_0 dt < r_c$ in order to incorporate the influence of interaction properly. We utilize scaled angular diffusion $D_\theta := 2D_r / \mu J$ and activity $Pe := v_0 / D_r r_c$ as control parameters to construct the phase diagram, delineating associated phases at a fixed dimensionless number density $\rho = N/L^2 = \rho_0$ with $\rho_0 r_c^2 = 0.4$.

The nematic order parameter is $\langle Q_{\alpha\beta} \rangle$ with $Q_{\alpha\beta}^{(i)} = (u_{i\alpha} u_{i\beta} - \frac{1}{d} \delta_{\alpha\beta})$ for i -th particle with α, β denoting the components. In 2D,

$$\mathbf{Q}^{(i)} = \frac{1}{2} \begin{pmatrix} \cos 2\theta_i & \sin 2\theta_i \\ \sin 2\theta_i & -\cos 2\theta_i \end{pmatrix}.$$

From numerical simulations, we assess the degree of nematic order by utilizing the positive eigenvalue of $\langle Q_{\alpha\beta} \rangle$, the scalar order parameter:

$$S = [\langle (\cos 2\theta_i) \rangle^2 + \langle (\sin 2\theta_i) \rangle^2]^{1/2}. \quad (4)$$

The value of S is bounded on both sides, $0 \leq S \leq 1$. To compute the steady-state average S across the entire system, we average over all N particles and further average over steady-state configurations, represented by red line points in Fig.1(b). Additionally, we determine the standard deviation of the global order parameter S and identify its maximum as the transition point D_θ^* for a given Pe ; these are indicated by blue line points in Fig.1(b). For a localized assessment of S , we perform averaging over particles within a local volume. This is used to determine S over coarse-grained volumes of linear dimension $10r_c$ to calculate the probability distributions $P(S)$ in Fig.1(c).

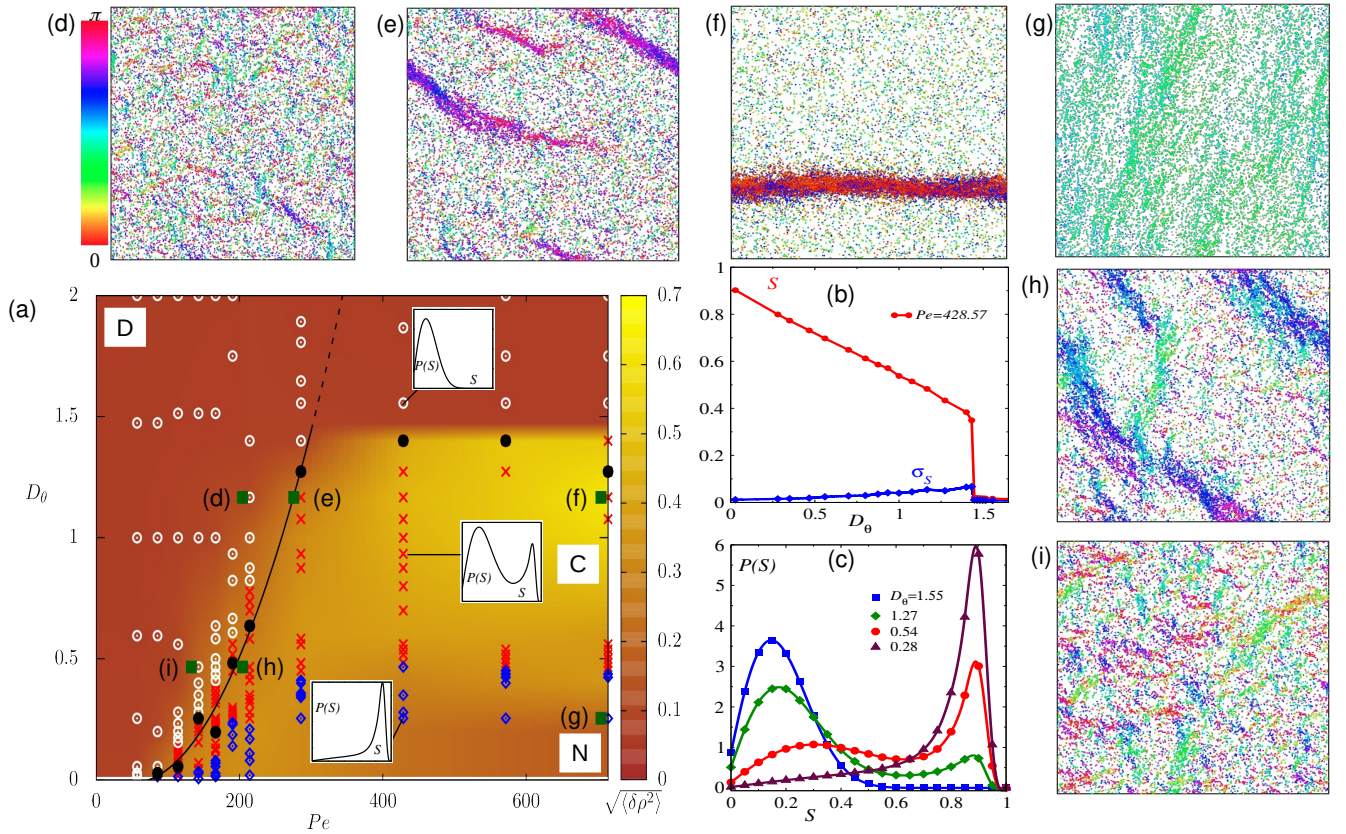


FIG. 1. (a) Phase diagram in (Pe, D_θ) plane with dimensionless activity $Pe = v_0/D_r r_c$ and orientational noise relative to alignment strength $D_\theta = 2D_r/\mu J$ showing three distinct regions: disordered (D), coexistence (C) and nematic (N). The solid black line has the scaling form $D_\theta^* \sim Pe^2$ (see Sec.4 for derivation). (b) The nematic order S (red line points) and standard deviation σ_s (blue line points) as a function of D_θ at a fixed $Pe = 428.57$. (c) The local probability distribution $P(S)$ at $Pe = 428.57$ and various D_θ mentioned in the figure legend. The distributions are calculated using S calculated over local coarse-grained volumes of linear dimension $10r_c$. (e-i) Representative configurations at parameter values marked by solid green boxes in the phase diagram in (a). The parameter values are $(Pe, D_\theta) = (142.85, 0.466)$, $(214.28, 0.466)$, $(714.28, 0.254)$, $(714.28, 1.166)$, $(285.71, 1.166)$, $(214.28, 1.166)$, respectively. The color palette to the left of Figure (d) denotes the heading directions of the particles in all the snapshots shown here.

3. Phase diagram

We begin our investigation by studying the steady states of the model in square geometry of size $L = 200$ and $N = 16000$, utilizing periodic boundary conditions (PBC). Fig.1(a) shows the phase diagram of the nematic-isotropic (NI) transition. The regions of the nematic phase (N) are denoted by blue diamonds, the region of nematic-isotropic coexistence (C) is indicated by red crosses, and the disordered isotropic phase (D) regions are marked by white open circles. The phase boundary between isotropic and coexistence is denoted by black-filled circles. The heat map in the phase diagram shows the amount of density fluctuations. This is calculated in coarse-grained volumes of linear dimension $10r_c$ using $\delta\rho = [\langle \rho^2 \rangle - \langle \rho \rangle^2]^{1/2}$, and then averaging over the system size and all steady state configurations. As the color codes show, the density fluctuation is maximum in the coexistence. Its presence is significant even in the or-

dered nematic phase. The fluctuation is minimal in the homogeneous isotropic phase.

The three insets show the typical distributions of the scalar nematic order parameter corresponding to nematic (N), coexistence (C), and isotropic (D) regions. An analytic description of the NI phase boundary $D_\theta \sim Pe^2$ is provided in the following section. Shown by a black solid line in Fig.1(a), it qualitatively captures the actual phase boundary up to $Pe \approx 300$. The broken solid line indicates a breakdown of this simple estimate. Beyond this point, the phase boundary becomes approximately independent of Pe . As expected, the active nematic phase is characterized by a giant number fluctuation [2, 29, 30]. For example, deep inside the nematic phase, at $Pe = 714.28$ and $D_\theta = 0.254$, the system shows $\langle \Delta n \rangle^2 = \langle n^2 \rangle - \langle n \rangle^2 \sim \langle n \rangle^a$ with $a \approx 1.52$; see Appendix-A. The steady-state pair correlation function $C(r) = 1 - b(r/L)^\alpha$ with $\alpha \approx 0.26$ [29] signifies a clear violation of Porod's law in the coexistence region. This cap-

tures a huge roughness of interfaces evidenced by large $(1-\alpha)$ characterizing a fluctuation-dominated phase separation [44].

The NI transition is captured using the dependence of the scalar order parameter S and its standard deviation $\sigma_s = [\langle S^2 \rangle - \langle S \rangle^2]^{1/2}$ on D_θ , at a fixed Pe ; see Fig.1(b). The cross-correlation between fluctuations in nematic order and density peaks near the transition, as detailed in Appendix-B. However, this correlation diminishes significantly within the nematic phase and approximately vanishes after transitioning to isotropic. The local probability distribution $P(S)$ in Fig.1(c) shows an unimodal distribution with the maximum at small S for large D_θ , transforms into a bimodal distribution at intermediate D_θ values. This clearly indicates a phase coexistence, characterizing a first-order transition. At an even smaller D_θ , the distribution becomes unimodal again, this time displaying a single maximum at large S , indicating a nematic phase.

Representative configurations are shown in Fig.1(d)-(i), with orientations distinguished by a color palette shown on the left of Fig.1(d). The parameter values associated with these configurations are marked by solid green squares on the phase diagram Fig.1(a). A typical configuration of the isotropic phase in Fig.1(d) shows an approximately homogeneous distribution of particles and their random orientations of heading direction. At a higher Pe , in Fig. 1(e), we observe a local clustering of particles in oriented bands. These bands display a higher nematic order. At an even higher Pe in Fig.1(f), simulations show system-spanning bands with large nematic order coexisting with a uniform isotropic background. This corresponds to the bimodal distribution in $P(S)$ shown in Fig.1(c). Decreasing D_θ , keeping Pe unchanged, in Fig.1(g), we observe nice nematic order all through the system, corresponding to a homogeneous nematic fluid phase. The corresponding distribution $P(S)$ is unimodal with the maximum at large S . Again, in Fig.1(h), we show a typical configuration at a smaller Pe and D_θ , near the phase boundary, to find local nematic bands coexisting with an isotropic background. At an even smaller Pe , the system gets back to the isotropic phase in the presence of large density fluctuations; see Fig.1(i).

4. Mean field and hydrodynamic analysis

Here, we consider the coupled evolution of the nematic order parameter density $\Pi_{ij}(\mathbf{r}, t) = Q_{ij}(\mathbf{r}, t)\rho(\mathbf{r}, t)$ and particle density $\rho(\mathbf{r}, t)$ [4, 10, 11, 20]. The local field of nematic order

$$\mathbf{Q}(\mathbf{r}, t) = \frac{S(\mathbf{r}, t)}{2} \begin{pmatrix} \cos 2\theta(\mathbf{r}, t) & \sin 2\theta(\mathbf{r}, t) \\ \sin 2\theta(\mathbf{r}, t) & -\cos 2\theta(\mathbf{r}, t) \end{pmatrix} \quad (5)$$

is determined by the local scalar order $S(\mathbf{r}, t)$ and orientation $\theta(\mathbf{r}, t)$. Using active current $J_i^{(a)} = -Pe \partial_j \Pi_{ji}$ [4], the particle density field evolves as,

$$\partial_t \rho = Pe \partial_i \partial_j \Pi_{ji} + D \nabla^2 \rho + \partial_i c_i, \quad (6)$$

where c_i denotes components of random current taken to be statistically isotropic and delta correlated, and D denotes the diffusion constant. The evolution of nematic order follows,

$$\begin{aligned} \partial_t \Pi_{ij} &= [\alpha_1 - \alpha_2 \text{Tr}(\Pi^2)] \Pi_{ij} + D \nabla^2 \Pi_{ij} \\ &+ \frac{Pe}{4} \left[\partial_i \partial_j - \frac{1}{2} \delta_{ij} \nabla^2 \right] \rho + q_{ij} \end{aligned} \quad (7)$$

where q_{ij} is an uncorrelated Gaussian tensorial noise, which is traceless and symmetric, denoting thermal or active fluctuations [4]. Here, the coefficients $\alpha_1 = [1 - D_\theta/D_\theta^{(c)}]$ and $\alpha_2 = (1/4)[D_\theta^{(c)}/D_\theta]^2$ with the equilibrium mean-field critical point $D_\theta^{(c)} = A\rho$ [29]; see Appendix-C.

In the homogeneous limit of constant ρ , Eq.(7) gives $\frac{dQ_{ij}}{dt} = [\alpha_1 - \alpha_2 \text{Tr}(Q^2)]Q_{ij}$ leading to a continuous transition at $\alpha_1 = 0$. Describing the first-order transition requires incorporating the density fluctuations [45, 46], for which we use a renormalized mean field theory [32, 47]. We consider a small activity-induced density fluctuation $\delta\rho$ such that $\rho = \rho_0 + \delta\rho$ to express $\alpha_{1,2}(\rho) = \alpha_{1,2}^0 + \alpha'_{1,2} \delta\rho$ where $\alpha_{1,2}^0 = \alpha_{1,2}(\rho_0)$ and $\alpha'_{1,2} = (\partial\alpha_{1,2}/\partial\rho)_{\rho_0}$. The requirement of a zero current steady state in density evolution suggests $\delta\rho \approx PeS/D$ [29]. Using this in the mean-field limit of Eq.(7), we obtain the evolution for scalar order

$$\partial_t S = [u_2 + u_3 S - u_4 S^2] S, \quad (8)$$

where, $u_2 = \alpha_1^0$, $u_3 = \alpha_1^0 Pe/D$ and $u_4 = \alpha_2^0$. This equation can be expressed as a free energy minimizing kinematics $\partial_t S = -\partial\mathcal{F}/\partial S$ with

$$\mathcal{F} = -\frac{u_2}{2} S^2 - \frac{u_3}{3} S^3 + \frac{u_4}{4} S^4, \quad (9)$$

keeping up to S^4 order term.

The cubic term in S in the effective free energy density \mathcal{F} results in a first-order NI transition. At the transition, the scalar order parameter jumps from $S = 0$ to

$$S_c = \frac{2}{3} \frac{\alpha_1^0 Pe}{\alpha_2^0 D}. \quad (10)$$

The transition point changes with Pe to give the transition line

$$D_\theta^* = D_\theta^{(c)} \left[1 + \frac{2}{9} \frac{(\alpha_1^0)^2}{\alpha_2^0} \left(\frac{Pe}{D} \right)^2 \right], \quad (11)$$

increasing quadratically with Pe . A plot of $D_\theta^* \sim Pe^2$ using the black solid line in Fig.1(a) approximately captures the phase boundary up to $D_\theta \approx 1.4$. At higher D_θ , even the activity-induced increased density fluctuations fail to sustain the nematic order, rendering the phase boundary independent of Pe . In fact, as can be observed from the heat map in Fig.1(a), the density fluctuation gets suppressed at these D_θ values. We note that the

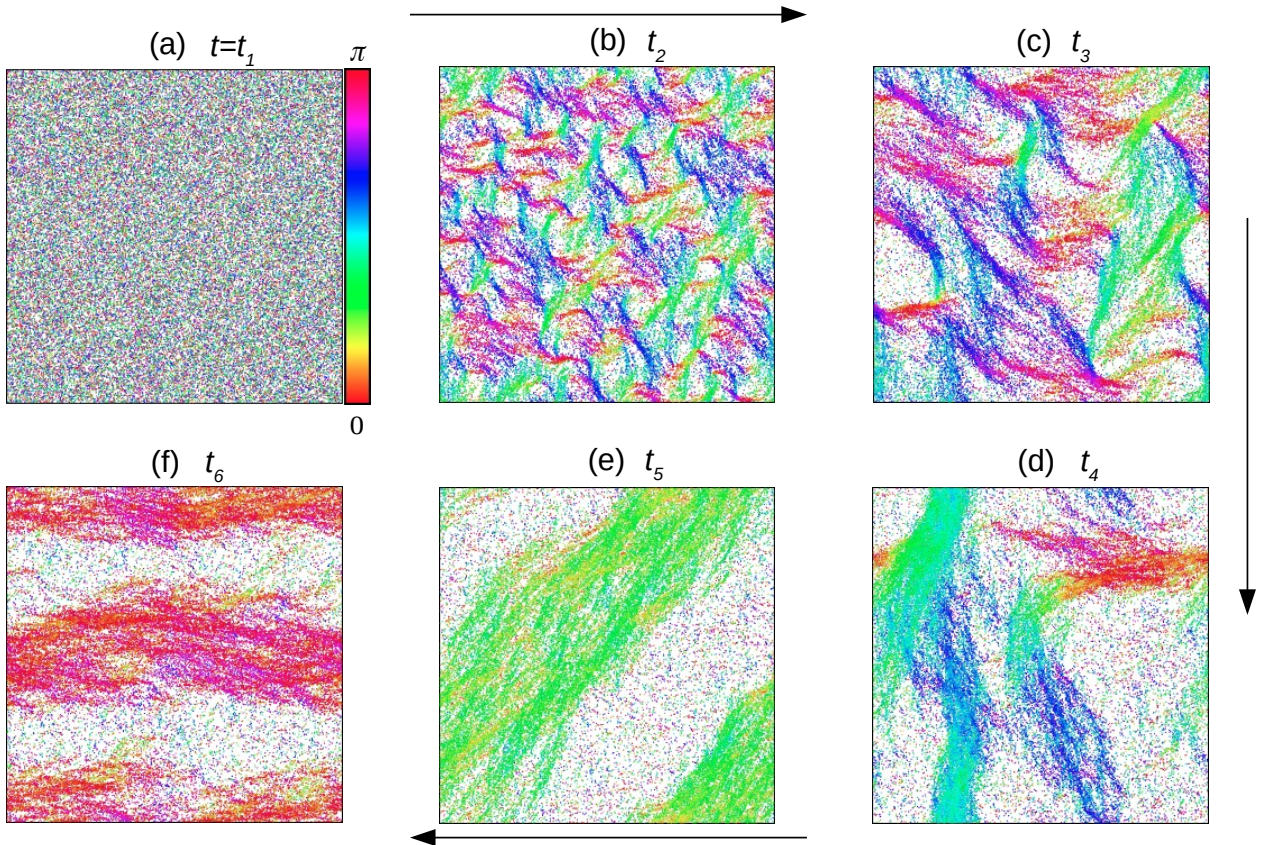


FIG. 2. Typical configurations corresponding to the evolution after a quench from $D_\theta = 2.8$ to $D_\theta = 0.28$ at $Pe = 428.57$ are shown. The color palette in (a) encodes orientations of particle heading directions. The black arrows show the direction of increasing time. At initial times, $t_1 = 0.007 D_r^{-1}$, the system is in a homogeneous disordered phase (a). By $t_2 = 2.8 D_r^{-1}$, thin nematic bands of higher density are formed. They are oriented in multiple directions (b). At a later time, $t_3 = 21 D_r^{-1}$, these bands coarsen into thicker and longer branched patterns (c). At an even later time $t_4 = 350 D_r^{-1}$, they coarsen into broader and system-spanning bands (d). By the time $t_5 = 12600 D_r^{-1}$, steady-state system-spanning nematic bands appear (e). These bands break, form, and orient along spontaneously chosen directions that vary with time. For example, see another steady-state configuration at $t_6 = 19600 D_r^{-1}$ (f). Here we use $N = 64000$, $Pe = 428.57$, $\rho r_c^2 = 0.4$, and $L = 400 r_c$.

first-order NI transition is purely active; it vanishes in the limit of $Pe \rightarrow 0$ with the vanishing of S_c .

Before closing this section, certain comments are in order. Within the Lebowhl-Lasher model used here, the first-order isotropic-nematic transition precludes the possible continuous transition as $D_\theta^* > D_\theta^{(c)}$. Moreover, the observed first-order transition relies crucially on the density dependence of $D_\theta^{(c)}$, which resulted from the reciprocal and additive nature of interaction implemented in the Lebowhl-Lasher model. If D_θ^* is independent of density, as in certain non-reciprocal models, the NI transition can become continuous [29].

5. Phase ordering kinematics

Having established the phenomenology of the NI transition, we now aim to understand the coarsening kinematics of the nematic order. Towards this end, we present our numerical results of the growth kinetics following a

deep quench at a fixed $Pe = 428.57$ from a homogeneous isotropic initial state at $D_\theta = 2.8$ to $D_\theta = 0.28$ corresponding to a steady-state nematic. For better statistics, we use a larger system with $N = 64000$. Fig.2 shows a typical series of snapshots depicting this evolution. As time progresses, domains of higher order parameters and higher density form, with their typical size increasing over time. The deep quench leads to local instability. In the beginning, the homogeneous isotropic state shows instability through the formation of nematically ordered filaments crisscrossing each other; see Fig.2(b). The small filaments merge and coarsen with time, as shown in Fig.2(c) and (d). At a late time, one finds dynamic system-spanning bands of nematically ordered regions; see Fig.2(e) and (f). In the steady state, the local undulations in nematic bands make them unstable toward breaking, and one finds repeated formation, breaking, and reorientations of such bands with time [11, 12].

To quantify these observations, we track the spatial nematic order parameter autocorrelation $C_{\mathbf{Q}}(r, t)$ and the

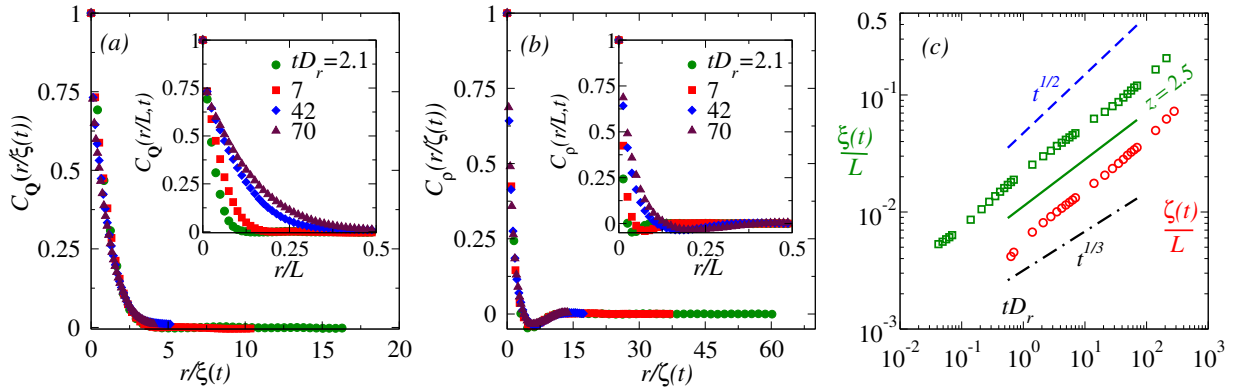


FIG. 3. The nematic and density autocorrelation $C_{\mathbf{Q}}(r)$ (a) and $C_{\rho}(r)$ (b) during quench from $D_{\theta} = 2.8$ to $D_{\theta} = 0.28$ at $Pe = 428.57$. Insets show the correlations plotted against r/L . The main plots show data collapse by scaling separation r by dynamic correlation lengths $\xi(t)$ (a) and $\zeta(t)$ (b). (c) The correlation lengths $\xi(t)$ (\square), $\zeta(t)$ (\circ) in the scaling regime exhibit similar power-law growths $\sim t^{1/z}$ with exponent $z \approx 2.5$, indicated by the solid green line. The growth exponent $2 < z < 3$ is shown using the dashed blue line of $t^{1/2}$ scaling and the dash-dotted black line of $t^{1/3}$ scaling. Cells of linear dimension $5r_c$ are used to calculate the coarse-grained correlations from numerical simulations.

density autocorrelation $C_{\rho}(r, t)$ as the system relaxes towards its final ordered state. To obtain a direct comparison against earlier field theory calculations, we divide the simulation volume into cells of length ℓ_c . We employ the coarse-grained order parameter $\mathbf{Q}(\mathbf{r}, t) = \frac{1}{n(t)} \sum_{i=1}^{n(t)} \mathbf{Q}^{(i)}$ by performing instantaneous averaging over local cells at positions \mathbf{r} containing $n(t)$ number of particles. Similarly, in the same cells, we use a coarse-grained local density $\rho(\mathbf{r}, t) = n(t)/\ell_c^2$. We use $\ell_c = 5r_c$ in the numerical calculations. The correlation functions are defined as follows:

$$C_{\mathbf{Q}}(r, t) = \frac{\text{Tr}\langle \mathbf{Q}(r, t) \mathbf{Q}(0, t) \rangle}{\text{Tr}\langle \mathbf{Q}^2(0, t) \rangle}, \quad (12)$$

and

$$C_{\rho}(r, t) = \frac{\langle \delta\rho(r, t) \delta\rho(0, t) \rangle}{\langle \delta\rho^2(0, t) \rangle} \quad (13)$$

where $\delta\rho(r) = \rho(r) - \rho_0$ and r denotes the separation between local coarse-grained volumes. For further details, see Appendix-D.

The time-dependent correlation functions plotted in Fig.3 are calculated averaging over forty independent trajectories. The simulations show exponentially decaying correlations up to $tD_r \approx 500$. Beyond that, the finite-size effect kicks in; the deep quench renders quasi-long ranged nematic order with power-law decay of correlations and system-spanning bands. At shorter times, the correlation length ℓ can be obtained by fitting the correlation functions with $\exp(-r/\ell)$ form. Rescaling the separations by correlation lengths $\ell = \xi(t)$ and $\ell = \zeta(t)$ for nematic and density correlations, we obtain nice data collapse for both the correlation functions, shown in the main figures of Fig.3(a) and (b).

In the intermediate time scaling regime, both the correlation lengths, $\zeta(t)$ and $\xi(t)$, increase algebraically. Note that the building up of orientational correlation precedes

that of local density; see the delay in growth of $\zeta(t)$ compared to $\xi(t)$ in Fig.3(c). This delay is caused by the time required for nematic instability to influence the density fluctuation. As can be seen from Eq.(6), the typical delay time is controlled by the quenched value of D_{θ} itself.

In the scaling regime, the correlation lengths grow following power laws $\xi(t) \sim t^{1/z_S}$ and $\zeta(t) \sim t^{1/z_{\rho}}$, with dynamic exponents $z_S, z_{\rho} \approx 2.5$; see Fig.3(c). It is interesting to note that earlier equilibrium simulations of a soft-spin version of the 2D Lebwohl-Lasher model led to an approximate phase ordering exponent $z_S \approx 2.5$ [48] differing from $\xi \propto (t/\ln t)^{1/2}$ growth law expected for equilibrium nematic [49]. In our simulations, the value of z_{ρ} is expected to be related to z_S due to the density-order coupling. Indeed, the bounds of non-conserved and conserved dynamics [50] to these exponents, $2 < z_S, z_{\rho} < 3$, are consistent with earlier non-stochastic hydrodynamic estimates [43]. A precise determination of the growth laws and growth exponents requires performing a more careful and extensive finite-size scaling procedure.

6. Outlook

We presented a comprehensive phase diagram as a function of activity Pe and relative orientational noise D_{θ} for the nematic-isotropic transition in dry active nematics with reciprocal alignment interaction. The additive nature of the interaction ensures a first-order transition via coupling of nematic order to density fluctuations, confirmed through a hydrodynamic theory and the corresponding mean-field arguments.

It is intriguing that despite zero macroscopic velocity, the phase behavior of these apolar SPPs shows intricate dependence on Pe . Our theoretical analysis predicts a phase boundary $D_{\theta} \sim Pe^2$, aligning well with simulation results up to $D_{\theta} \approx 1.4$. Beyond this, local density in-

creases are not enough to sustain nematic order, resulting in a Pe -independent phase boundary. The scalar order parameter shows a discontinuous jump proportional to Pe at the transition, disappearing in the passive particle limit of vanishing Pe . We identified a broad parameter regime of phase coexistence. Deep within the nematic phase, the nematic bands are inherently unstable, exhibiting giant fluctuations and turbulent dynamics due to their continuous formation and breakup.

Moreover, we investigated phase ordering kinetics by quenching from the isotropic to the nematic phase. This revealed coarsening patterns with correlation lengths in nematic order and density fluctuations growing as $t^{1/z}$ with exponents, $z_S, z_\rho \approx 2.5$ remaining within the bounds of non-conserved and conserved dynamics, $2 < z_S, z_\rho < 3$, a range consistent with earlier hydrodynamic predictions in Ref. [43]. The quench in scaled orientational coupling showed a lag in particle clustering relative to the growth of nematic correlation.

In conclusion, we obtained a comprehensive phase diagram for reciprocal alignment in active nematics, supported by mean-field predictions for the observed transition and phase boundaries. A theoretical description beyond the mean field explaining the full phase diagram will require further work. The numerical studies of coarsening dynamics revealed dynamic exponents with values in between the exponents for non-conserved and conserved dynamics. A precise numerical determination of growth laws requires careful system size scaling studies. The extent to which the observed phenomenology holds for non-reciprocal interactions warrants further investigation.

Author Contributions

DC designed and supervised the research. AS performed all the numerical calculations and data analysis. DC and AS wrote the manuscript.

Acknowledgments

The numerical simulations were performed using SAMKHYA, the High-Performance Computing Facility provided by the Institute of Physics, Bhubaneswar. D.C. thanks Sriram Ramaswamy and Abhishek Chaudhuri for useful discussions and acknowledges the Department of Atomic Energy, Government of India (1603/2/2020/IoP/R&D-II/150288) and the International Centre for Theoretical Sciences (ICTS-TIFR), Bangalore, for an Associateship.

A. Giant number fluctuations

Deep inside the nematic phase, at $Pe = 714.28$ and $D_\theta = 0.254$, we analyze the particle number fluctuations $\langle \Delta n^2 \rangle = \langle n^2 \rangle - \langle n \rangle^2$ as a function of $\langle n \rangle$; see Fig.4.

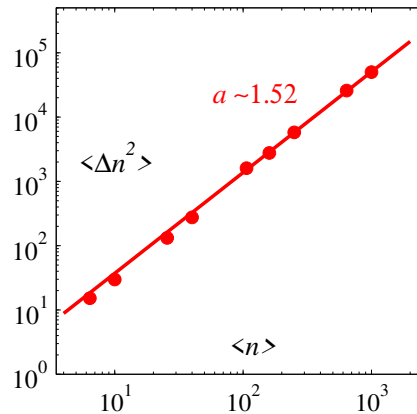


FIG. 4. The number fluctuation $\langle \Delta n^2 \rangle$ as a function of mean number $\langle n \rangle$ at $Pe = 714.28$ and $D_\theta = 0.254$, calculated over square coarse graining areas of linear dimension $\ell_c/r_c = 4, 5, 8, 10, 16, 20, 25, 40, 50$. A fitting, the solid line, shows $\langle \Delta n^2 \rangle \sim \langle n \rangle^a$, with $a \approx 1.52$.

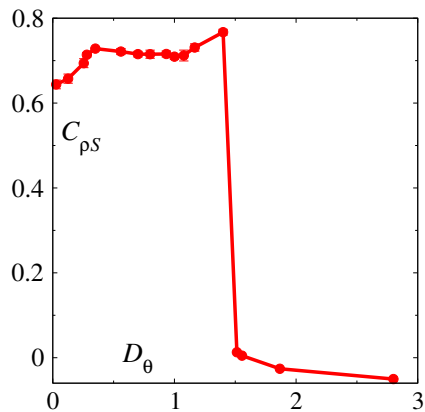


FIG. 5. Cross-correlation coefficient $C_{\rho S}$ with the scaled orientation noise D_θ at a fixed $Pe = 428.57$.

This shows giant number fluctuations, characterized by $\langle \Delta n^2 \rangle \sim \langle n \rangle^a$, with $a \approx 1.52 > 1$ but less than $a = 2$ predicted in [2] and found by numerical simulations in [30, 31]. See Fig.1(g) for a typical configuration corresponding to these parameter values.

B. Density-nematic order cross correlation

Here, we compute the cross-correlation $C_{\rho S} = \langle \delta \rho(r) \delta S(r) \rangle / \sigma_S \sigma_\rho$, where $\delta \rho(r) = \rho(r) - \langle \rho \rangle$ and $\delta S(r) = S(r) - \langle S \rangle$ with $\langle \rho \rangle$ and $\langle S \rangle$ denoting the mean density and mean scalar order, respectively (see Fig.5). Further, $\sigma_S = \langle \delta S^2(r) \rangle^{1/2}$ and $\sigma_\rho = \langle \delta \rho^2(r) \rangle^{1/2}$ denote the standard deviations of nematic and density fields. The calculations are performed over coarse-grained cells of linear dimension $10 r_c$. In the disordered phase, $D_\theta > 1.5$, the cross-correlation $C_{\rho S}$ is slightly negative, indicating an anti-correlation between the fields. This happens because an increase in randomly oriented elements within

a coarse-grained region can lead to better cancellation in averaging and reduce the overall nematic order. Near the transition point, $D_\theta \approx 1.4$, $C_{\rho S}$ reaches its positive maximum because higher particle density in bands enhances order, while the low-density background remains disordered (see Fig.1(f)). Deeper in the nematic phase, $D_\theta \lesssim 0.28$, $C_{\rho S}$ decreases as regions of both high and low densities exhibit similar nematic order (see Fig. 1(g)).

C. Equilibrium mean-field theory for nematic-isotropic transition

Using Eq.(2) it is straightforward to write the mean-field Fokker-Planck equation for orientation [23, 29]

$$\partial_t p(\theta, t) = \partial_\theta \left[\gamma(n) \int_0^{2\pi} d\theta' \sin[2(\theta - \theta')] p(\theta, t) p(\theta', t) \right] + D_r \partial_\theta^2 p, \quad (\text{C1})$$

where $\gamma(n) = 2\mu J n$, with $n = \pi r_c^2 \rho$ denoting the mean number of nearest neighbors. The steady-state solution is

$$p_{st}(\theta) = \mathcal{N} \exp \left[\frac{\gamma(n) S}{2D_r} \cos(2(\theta - \psi)) \right]. \quad (\text{C2})$$

where

$$S = \left| \int_0^{2\pi} d\theta p_{st}(\theta) \exp(i 2\theta) \right| \quad (\text{C3})$$

denotes the scalar order parameter quantifying the degree of nematic order, and ψ denotes the direction of broken symmetry.

From equations (C3) and (C2) we find the self-consistency relation $S = I_1 \left[\frac{\gamma(n) S}{2D_r} \right] / I_0 \left[\frac{\gamma(n) S}{2D_r} \right]$, where $I_n[\cdot]$ denotes n -th order modified Bessel function of the first kind. For small S , a Taylor expansion gives, $S \approx \frac{\gamma(n) S}{4D_r} \left(1 - \frac{\gamma^2(n) S^2}{64D_r^2} \right)$. Above the transition point, only one solution exists, $S = 0$. Below it, $S = (2D_\theta / D_\theta^{(c)}) (1 - D_\theta / D_\theta^{(c)})^{1/2}$ where we used $D_\theta = 2D_r / \mu J$ and the critical point

$$D_\theta^{(c)} = n = \pi r_c^2 \rho \quad (\text{C4})$$

The above relations can be used to obtain an approximate mean-field evolution of the scalar order $dS/dt = -\partial \mathcal{A} / \partial S$ with [50]

$$\mathcal{A} = -\frac{\alpha_1}{2} S^2 + \frac{\alpha_2}{4} S^4 \quad (\text{C5})$$

where $\alpha_1 = 1 - \frac{D_\theta}{D_\theta^{(c)}}$ and $\alpha_2 = \frac{1}{4} \left(\frac{D_\theta^{(c)}}{D_\theta} \right)^2$, with $D_\theta^{(c)} = A\rho$.

D. Coarse-grained correlations

Using the expression of $\mathbf{Q}(\mathbf{r}, t)$ in Eq.(5), we get the following expressions for the coarse-grained quantities, $S^2(\mathbf{r}, t) = S_1^2(\mathbf{r}, t) + S_2^2(\mathbf{r}, t)$ and $\tan 2\theta(\mathbf{r}, t) = S_2(\mathbf{r}, t) / S_1(\mathbf{r}, t)$ with $S_1(\mathbf{r}, t) = \langle \cos 2\theta(\mathbf{r}, t) \rangle = \frac{1}{n(t)} \sum_{i=1}^{n(t)} \cos 2\theta_i$ and $S_2(\mathbf{r}, t) = \langle \sin 2\theta(\mathbf{r}, t) \rangle = \frac{1}{n(t)} \sum_{i=1}^{n(t)} \sin 2\theta_i$. Here, $n(t)$ denotes the instantaneous number of particles in the coarse-grained volume around \mathbf{r} . Therefore, the coarse-grained nematic correlation finally gets the form,

$$C_{\mathbf{Q}}(r, t) = \frac{\langle S(\mathbf{r}_1, t) S(\mathbf{r}_2, t) \cos [2\theta(\mathbf{r}_1, t) - 2\theta(\mathbf{r}_2, t)] \rangle}{\langle S^2(0, t) \rangle}, \quad (\text{D1})$$

where $r = |\mathbf{r}_1 - \mathbf{r}_2|$.

The correlation lengths are obtained by fitting the numerically calculated correlation functions with exponential decay of form $\exp(-r/\ell)$ with ℓ denoting the correlation length. Beyond the scaling regime shown in Fig.3, the nematic order grows quickly to span the whole system and changes from exponential to power-law decay, characteristic of the steady-state 2D active nematic phase. Related to this, the density correlation length also saturates. This crossover is entirely a finite-size effect, shifting to a later time and larger length scales in bigger systems. The data for this crossover is not shown explicitly in Fig.3.

-
- [1] R. Aditi Simha and Sriram Ramaswamy. Hydrodynamic fluctuations and instabilities in ordered suspensions of self-propelled particles. *Phys. Rev. Lett.*, 89(5):058101, 2002.
- [2] S. Ramaswamy, R. Aditi Simha, and J. Toner. Active nematics on a substrate: Giant number fluctuations and long-time tails. *Europhysics Letters*, 62(2):196, apr 2003.
- [3] Sriram Ramaswamy. The Mechanics and Statistics of Active Matter. *Annu. Rev. Condens. Matter Phys.*,

- 1(1):323–345, aug 2010.
- [4] M. C. Marchetti, J. F. Joanny, S. Ramaswamy, T. B. Liverpool, J. Prost, Madan Rao, and R. Aditi Simha. Hydrodynamics of soft active matter. *Rev. Mod. Phys.*, 85(3):1143–1189, jul 2013.
- [5] Sriram Ramaswamy. Active fluids. *Nat. Rev. Phys.*, 1(11):640–642, oct 2019.
- [6] M. Reza Shaebani, Adam Wysocki, Roland G. Winkler, Gerhard Gompper, and Heiko Rieger. Computational

- models for active matter. *Nat. Rev. Phys.*, 2(4):181–199, apr 2020.
- [7] F Julicher, K Kruse, J Prost, and J Joanny. Active behavior of the Cytoskeleton. *Phys. Rep.*, 449(1-3):3–28, sep 2007.
- [8] J Prost, F Jülicher, and J-f Joanny. Active gel physics. *Nat. Phys.*, 11(2):111–117, feb 2015.
- [9] Clemens Bechinger, Roberto Di Leonardo, Hartmut Löwen, Charles Reichhardt, Giorgio Volpe, and Giovanni Volpe. Active Particles in Complex and Crowded Environments. *Rev. Mod. Phys.*, 88(4):045006, nov 2016.
- [10] Xia-qing Shi and Yu-qiang Ma. Deterministic endless collective evolution in active nematics. *preprint arXiv:1011.5408*, 2010.
- [11] Xia-qing Shi, Hugues Chaté, and Yu-qiang Ma. Instabilities and chaos in a kinetic equation for active nematics. *New J. Phys.*, 16(3):035003, mar 2014.
- [12] Sandrine Ngo, Anton Peshkov, Igor S Aranson, Eric Bertin, Francesco Ginelli, and Hugues Chaté. Large-scale chaos and fluctuations in active nematics. *Physical review letters*, 113(3):038302, 2014.
- [13] Biplob Bhattacharjee and Debasish Chaudhuri. Re-entrant phase separation in nematically aligning active polar particles. *Soft Matter*, 15(42):8483–8495, 2019.
- [14] Tamás Vicsek, András Czirók, Eshel Ben-Jacob, Inon Cohen, and Ofer Shochet. Novel type of phase transition in a system of self-driven particles. *Physical Review Letters*, 75(6):1226, 1995.
- [15] Guillaume Grégoire and Hugues Chaté. Onset of Collective and Cohesive Motion. *Phys. Rev. Lett.*, 92(2):025702, jan 2004.
- [16] H. Chaté, F. Ginelli, G. Grégoire, F. Peruani, and F. Raynaud. Modeling collective motion: Variations on the Vicsek model. *Eur. Phys. J. B*, 64(3-4):451, 2008.
- [17] John Toner and Yuhai Tu. Long-range Order in a 2d dynamic xy model: how birds fly together. *Phys. Rev. Lett.*, 75(23):4326–4329, 1995.
- [18] Fernando Peruani, Andreas Deutsch, and Markus Bär. Nonequilibrium clustering of self-propelled rods. *Phys. Rev. E*, 74(3):030904, sep 2006.
- [19] Francesco Ginelli, Fernando Peruani, Markus Bär, and Hugues Chaté. Large-scale collective properties of self-propelled rods. *Physical review letters*, 104(18):184502, 2010.
- [20] Eric Bertin, Hugues Chaté, Francesco Ginelli, Shradha Mishra, Anton Peshkov, and Sriram Ramaswamy. Mesoscopic theory for fluctuating active nematics. *New J. Phys.*, 15(8):085032, aug 2013.
- [21] Daniel L. Blair, T. Neicu, and A. Kudrolli. Vortices in vibrated granular rods. *Phys. Rev. E*, 67:031303, Mar 2003.
- [22] Vijay Narayan, Sriram Ramaswamy, Narayanan Menon, The Caspt, and The Caspt. Long-Lived Giant Number Fluctuations. *Science (80-.)*, 317(July):105–108, 2007.
- [23] Oleksandr Chepizhko, David Saintillan, and Fernando Peruani. Revisiting the emergence of order in active matter. *Soft Matter*, 17(11):3113–3120, 2021.
- [24] Dirk Helbing, Illés Farkas, and Tamás Vicsek. Simulating dynamical features of escape panic. *Nature*, 407(6803):487–490, sep 2000.
- [25] Suropriya Saha, Jaime Agudo-Canalejo, and Ramin Golestanian. Scalar Active Mixtures: The Nonreciprocal Cahn-Hilliard Model. *Phys. Rev. X*, 10(4):41009, 2020.
- [26] A. V. Ivlev, J. Bartnick, M. Heinen, C. R. Du, V. Nosenko, and H. Löwen. Statistical mechanics where Newton’s third law is broken. *Phys. Rev. X*, 5(1):011035, 2015.
- [27] Michel Fruchart, Ryo Hanai, Peter B. Littlewood, and Vincenzo Vitelli. Non-reciprocal phase transitions. *Nature*, 592(7854):363–369, apr 2021.
- [28] Sarah A. M. Loos, Sabine H. L. Klapp, and Thomas Martynec. Long-range Order and Directional Defect Propagation in the Nonreciprocal XY Model with Vision Cone Interactions. *Phys. Rev. Lett.*, 130(19):198301, 2022.
- [29] Arpan Sinha and Debasish Chaudhuri. How reciprocity impacts ordering and phase separation in active nematics? *Soft Matter*, 20(i):788–795, 2024.
- [30] Shradha Mishra and Sriram Ramaswamy. Active Nematics Are Intrinsically Phase Separated. *Phys. Rev. Lett.*, 97(9):090602, aug 2006.
- [31] Hugues Chaté, Francesco Ginelli, and Raúl Montagne. Simple model for active nematics: Quasi-long-range order and giant fluctuations. *Physical review letters*, 96(18):180602, 2006.
- [32] Rakesh Das, Manoranjan Kumar, and Shradha Mishra. Order-disorder transition in active nematic: A lattice model study. *Sci. Rep.*, 7(1):7080, aug 2017.
- [33] Fernando Peruani, Jörn Starruß, Vladimir Jakovljevic, Lotte Sogaard-Andersen, Andreas Deutsch, and Markus Bär. Collective Motion and Nonequilibrium Cluster Formation in Colonies of Gliding Bacteria. *Phys. Rev. Lett.*, 108(9):098102, feb 2012.
- [34] Hans Gruler, Manfred Schienbein, Kurt Franke, and Anne de Boisfleury-chevance. Migrating Cells: Living Liquid Crystals. *Mol. Cryst. Liq. Cryst. Sci. Technol. Sect. A. Mol. Cryst. Liq. Cryst.*, 260(1):565–574, feb 1995.
- [35] H Gruler, U Dewald, and M Eberhardt. Nematic liquid crystals formed by living amoeboid cells. *The European Physical Journal B-Condensed Matter and Complex Systems*, 11:187–192, 1999.
- [36] Lakshmi Balasubramaniam, René-Marc Mège, and Benoît Ladoux. Active nematics across scales from cytoskeleton organization to tissue morphogenesis. *Curr. Opin. Genet. Dev.*, 73:101897, apr 2022.
- [37] Yilin Wu, A. Dale Kaiser, Yi Jiang, and Mark S. Alber. Periodic reversal of direction allows Myxobacteria to swarm. *Proc. Natl. Acad. Sci.*, 106(4):1222–1227, jan 2009.
- [38] Matthias Theves, Johannes Taktikos, Vasily Zaburdaev, Holger Stark, and Carsten Beta. A Bacterial Swimmer with Two Alternating Speeds of Propagation. *Biophys. J.*, 105(8):1915–1924, oct 2013.
- [39] Jörn Starruß, Fernando Peruani, Vladimir Jakovljevic, Lotte Sogaard-Andersen, Andreas Deutsch, and Markus Bär. Pattern-formation mechanisms in motility mutants of *Myxococcus xanthus*. *Interface Focus*, 2(6):774–785, dec 2012.
- [40] Greg M Barbara and James G Mitchell. Bacterial tracking of motile algae. *FEMS Microbiol. Ecol.*, 44(1):79–87, may 2003.
- [41] Barry L. Taylor and D. E. Koshland. Reversal of Flagellar Rotation in Monotrichous and Peritrichous Bacteria: Generation of Changes in Direction. *J. Bacteriol.*, 119(2):640–642, aug 1974.
- [42] P. A. Lebowhl and G. Lasher. Nematic-liquid-crystal order—a monte carlo calculation. *Phys. Rev. A*, 6:426–429, Jul 1972.

- [43] Shradha Mishra, Sanjay Puri, and Sriram Ramaswamy. Aspects of the density field in an active nematic. *Philosophical Transactions of the Royal Society A: Mathematical, Physical and Engineering Sciences*, 372(2029):20130364, 2014.
- [44] Dibyendu Das and Mustansir Barma. Particles Sliding on a Fluctuating Surface: Phase Separation and Power Laws. *Phys. Rev. Lett.*, 85(8):1602–1605, aug 2000.
- [45] Jing-Huei Chen, T. C. Lubensky, and David R. Nelson. Crossover near fluctuation-induced first-order phase transitions in superconductors. *Phys. Rev. B*, 17(11):4274–4286, jun 1978.
- [46] B. I. Halperin, T. C. Lubensky, and Shang-keng Ma. First-Order Phase Transitions in Superconductors and Smectic-A Liquid Crystals. *Phys. Rev. Lett.*, 32(6):292–295, feb 1974.
- [47] Wei-Lin Tu. *Renormalized Mean Field Theory*, pages 21–31. Springer Singapore, Singapore, 2019.
- [48] R. E. Blundell and A. J. Bray. Phase-ordering dynamics of nematic liquid crystals. *Phys. Rev. A*, 46(10):6154–6157, 1992.
- [49] Alan J Bray. Theory of phase-ordering kinetics. *Advances in Physics*, 51(2):481–587, 2002.
- [50] P. M. Chaikin and T. C. Lubensky. *Principles of Condensed Matter Physics*. Cambridge University Press, Cambridge, jun 1995.